Chapter – 3

Si-B-C-N Ceramics Derived from MW-33 Precursor

For the preparation of MW-33 derived Si-B-C-N ceramics, see Section 2.1 (Chapter 2). For crystallization such ceramics were annealed at 1800 °C under the following conditions: (i) 1 h, 1 MPa N_2 (sample **I**), (ii) 3 h, 1 MPa N_2 (sample **II**), (iii) 1 h, 10 MPa N_2 (sample **III**), and (iv) 3 h, 10 MPa N_2 (sample **IV**). For comparison, the creep behavior was also studied of as-thermolyzed material. Therefore, experimental data will also be provided for an amorphous Si-B-C-N ceramic (sample **V**), which reflects the state after thermolysis of the green body at 1400 °C.

3.1 Results

3.1.1 Structural Characterization

(i) X-ray diffraction (XRD)

The X-ray diffraction diagrams of the Si-B-C-N ceramics obtained from samples annealed at 1800 °C for different holding times and nitrogen pressures are given in Figure 3.1.

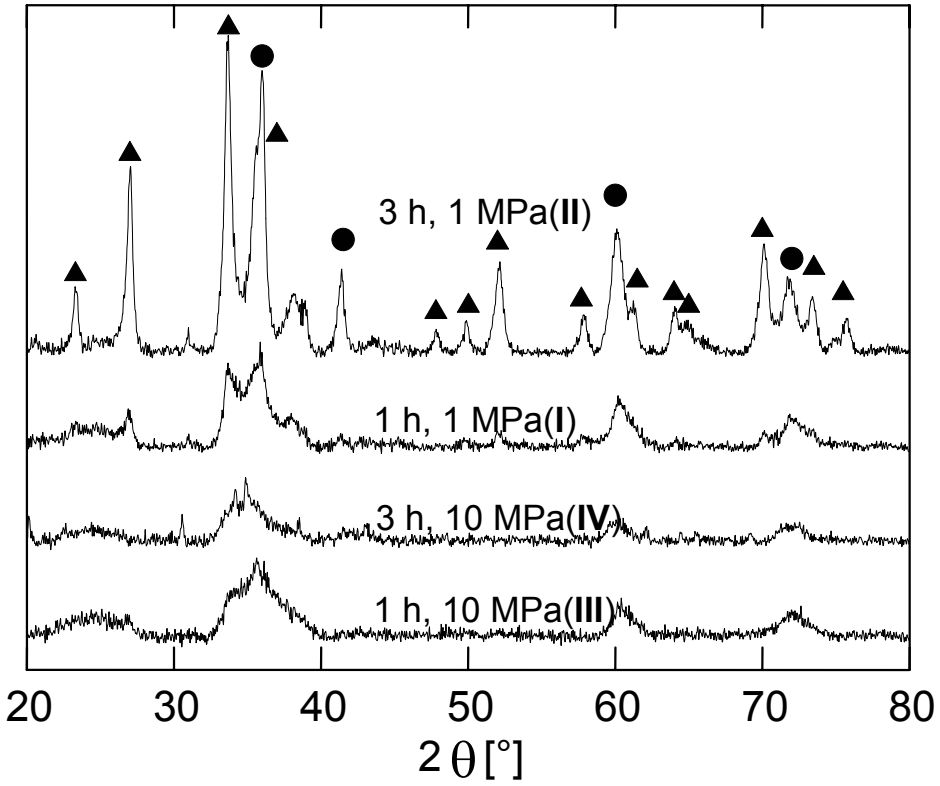

Figure: 3.1 XRD patterns for Si-B-C-N ceramics annealed at 1800 °C with various holding times and N_2-pressures (● = α/β-SiC, ▲ = β-Si_3N_4).

They reflect a considerable influence of the nitrogen pressure on the crystallization of the amorphous Si-B-C-N ceramics. Obviously, an increased nitrogen pressure of 10 MPa retards the crystallization process. Here, the samples almost regardless of the annealing time of 1 or 3 h (samples **III** and **IV**) exhibit mainly broad peaks at 2θ = 36°, 60.5°, and 72° which can be related to silicon carbonitride domains. If during the annealing process a lower nitrogen pressure of 1 MPa is applied, then additional peaks due to the formation of silicon carbide and silicon nitride are visible. At a holding time of 1 h (sample **I**) only relatively weak and broad diffraction signals show up. An extension of the holding time to 3 h, however, results in a considerable sharpening of all reflections along with a substantial increase of the peak intensities (sample **II**).

(ii) Transmission electron microscopy (TEM)

The bright-field TEM images of crystalline Si-B-C-N ceramics, obtained at nitrogen pressures of 1 and 10 MPa, are presented in Figure 3.2.

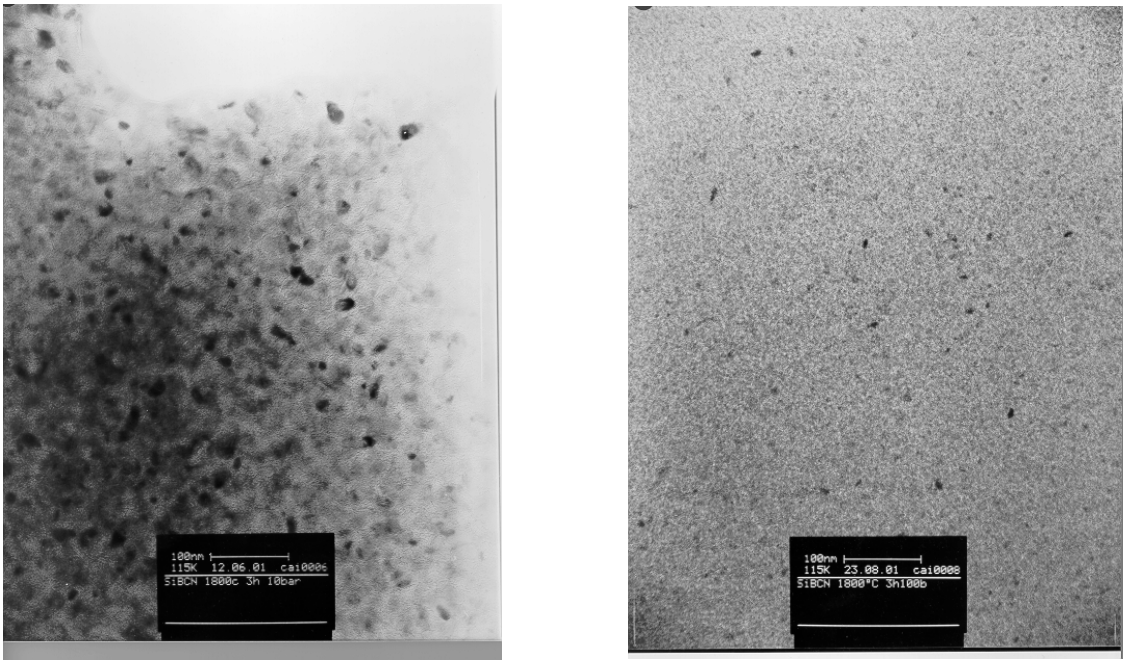

(a) **(b)**

Figure: 3.2 TEM of nano-crystalline Si-B-C-N ceramic crystallized at (a) 1800 °C, 3 h - 1 MPa N_2 pressure (Sample II) (b) 1800 °C, 3 h - 10 MPa N_2 pressure (Sample IV).

The TEM image of the specimen **II**, obtained with the annealing conditions 1800°C, 3 h and 1 MPa N_2 (Figure 3.2 (a)), clearly proves the formation of SiC and Si_3N_4 nanocrystallites. The mean crystallite size is around 30 nm for specimen **II**. The TEM image shown in Figure 3.2 (b) from the sample annealed at a higher nitrogen pressure of 10 MPa (sample **IV**). It reflects a predominantly amorphous character of that annealed ceramic, in close agreement with the findings from the X-ray diffraction experiments (see above, Figure 3.1).

(iii) Solid state NMR studies

The experimental results on the NMR studies of the annealed ceramics derived from boron-modified polyhydridovinylsilazane are summarized in Figure 3.3. The ^{13}C NMR spectra of these materials are given in the left column of Figure 3.3. The upper spectrum, referring to sample **I** (annealing time: 1 h, nitrogen pressure: 1 MPa) exhibits two major signals at around 120 and 20 ppm, which – according to previous studies on boron-modified polysilazanes [98Sch, 01Sch] – can be attributed to amorphous (graphite-like) carbon (SP^2-C) and $\mathbf{C}H_xSi_{4-x}$ (SP^3-C) units (x = 0, 1 or 2), respectively. A longer annealing time of 3 h (sample **II**) at the same nitrogen pressure gives rise to a ^{13}C NMR spectrum (second spectrum from top) with a single peak of SP^3-C. The ^{13}C NMR spectrum for the sample annealed for 1 h at a nitrogen pressure of 10 MPa (sample **III**) again contains both signals at 120 and 20 ppm, as discussed for sample **I**. In the case of 3 h annealing at a nitrogen pressure of 10 MPa (sample **III**) no ^{13}C NMR signals could be detected which, however, is not unusual. Former NMR studies on such precursor-derived ceramics have shown that in general ^{13}C NMR spectra not so easy to detect at annealing temperatures above 1100 °C [98Sch, 01Sch]. The ^{13}C NMR spectra shown here therefore represent a few cases, where it was nevertheless possible to get ^{13}C NMR signal of reasonable quality.

The corresponding ^{29}Si NMR spectra are given in the second column of Figure 3.3. An inspection of these spectra reveals that, independent of the particular annealing conditions,

two signals can be registered at -18 and -48 ppm, which are attributed to the formation of $\underline{Si}C_4$ (β-SiC: -20 ppm [87Har]) and $\underline{Si}N_4$ units (Si_3N_4: -48 ppm [87Car]), respectively. The relative magnitudes and widths of these signals, however, vary with the actual annealing conditions. It is quite obvious that the ^{29}Si NMR signals from samples **I** and **II** annealed at a lower nitrogen pressure of 1 MPa are better resolved than those obtained after treatment at higher pressure. Likewise, the relative signal intensity of the $\underline{Si}N_4$ units is found to increase with increasing nitrogen pressure, and decreasing annealing time, whereas the signal intensity of the $\underline{Si}C_4$ units displays the opposite behavior.

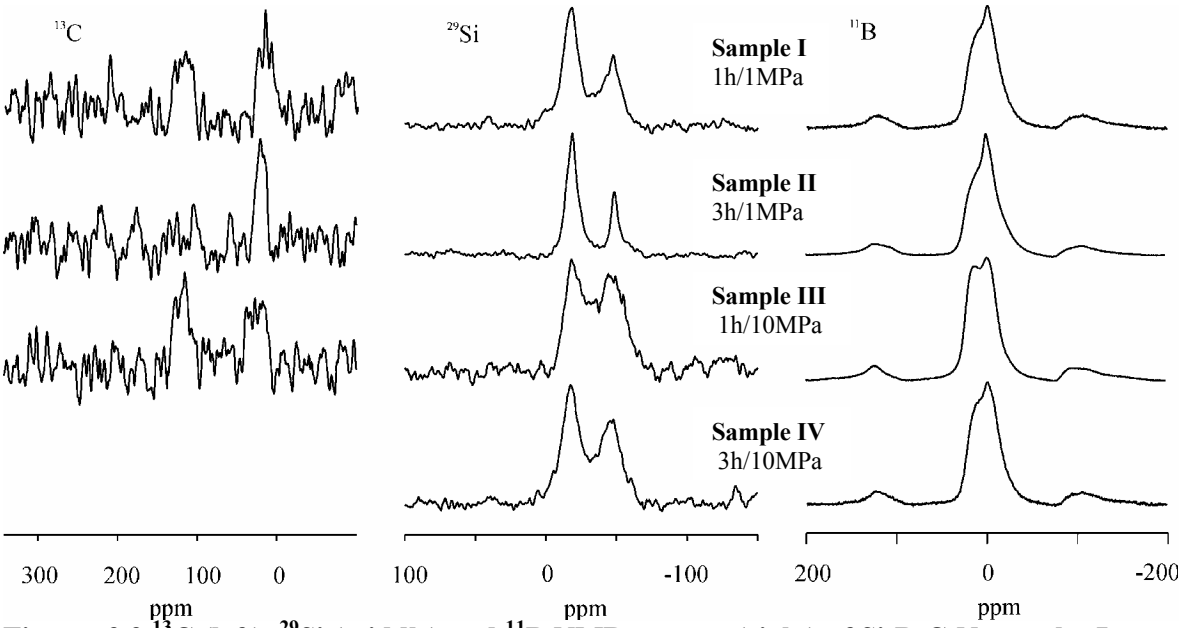

Figure: 3.3 ^{13}C (left), ^{29}Si (middle) and ^{11}B NMR spectra (right) of Si-B-C-N samples I to IV, annealed at 1800 °C with the conditions (holding time, N_2 pressure) described in the text.

The signals derived from the samples annealed at the higher nitrogen pressure clearly show an increased intensity in between the two peaks of $\underline{Si}C_4$ and $\underline{Si}N_4$ which correspond to mixed coordinated silicon atoms like SiC_3N, SiC_2N_2 and/or $SiCN_3$ most typical for the amorphous state of such materials. According to these data the sample annealed only for 1 h contains the highest content of amorphous phase.

The experimental ^{11}B NMR spectra are displayed in the right column of Figure 3.3. These spectra consist of two components: (i) a broad spectral component with a second-order

quadrupolar broadening, which is typical for trigonally coordinated boron atoms i.e., $\underline{B}N_3$ units [91Mar] as in hexagonal boron nitride, and (ii) a second, isotropic signal at 0 ppm which can be attributed to tetragonally co-ordinated boron atoms ($\underline{B}N_4$ units [91Mar]). The former component is obviously distinct in the ^{11}B NMR spectrum of sample **III** (annealing conditions: 1 h/ 10 MPa N_2). The isotropic component is found to increase with increasing annealing time and upon lowering the nitrogen pressure.

3.1.2 Microstructure

Microstructual characterization studies reveal that the annealed materials contain still more or less amorphous phase and the microstructures are characterized by small crystallites which are embedded in a matrix phase which is amorphous. The highest amount of crystallinity was recorded for sample **II**, with a mean crystallite size of around 30 nm. Quantification of the amount of crystalline phases against the amorphous part was difficult, hence no information on the amount of crystalline phases present in the material is provided here. Beside these general features of the microstructure, it contains pores and frequently crystallites which differ in morphology and location. Figure 3.4 shows the morphology and distribution of pores in all the annealed materials. The average pore size in the materials were found to be in the order of 10 μm. This comes from the fact that these materials were produced from a wide range of polymer particles (see Table 2.2), which facilitate the formation of more compact bodies.

(i) Crystallization in bulk

Crystallization behavior of materials synthesized at low and high nitrogen pressures was studied by transmission electron microscopy in detail [01Cai, 02Cai]. The observations reveal that increasing nitrogen overpressure results in retardation of the crystallization processes, but individual large crystallites of a new Si_3N_4 phase distinctive from α and β - Si_3N_4 were found

dispersed along with SiC and Si_3N_4. These individual large crystallites possess a hexagonal structure with lattice parameters a = 0.737 nm and c = 0.536 nm. Since the structure and lattice parameters of the observed phase are close to α - Si_3N_4, it can be considered as a variant of the α - Si_3N_4 phase. The crystallites were only found with high nitrogen pressure and occur only frequently in sample **IV**.

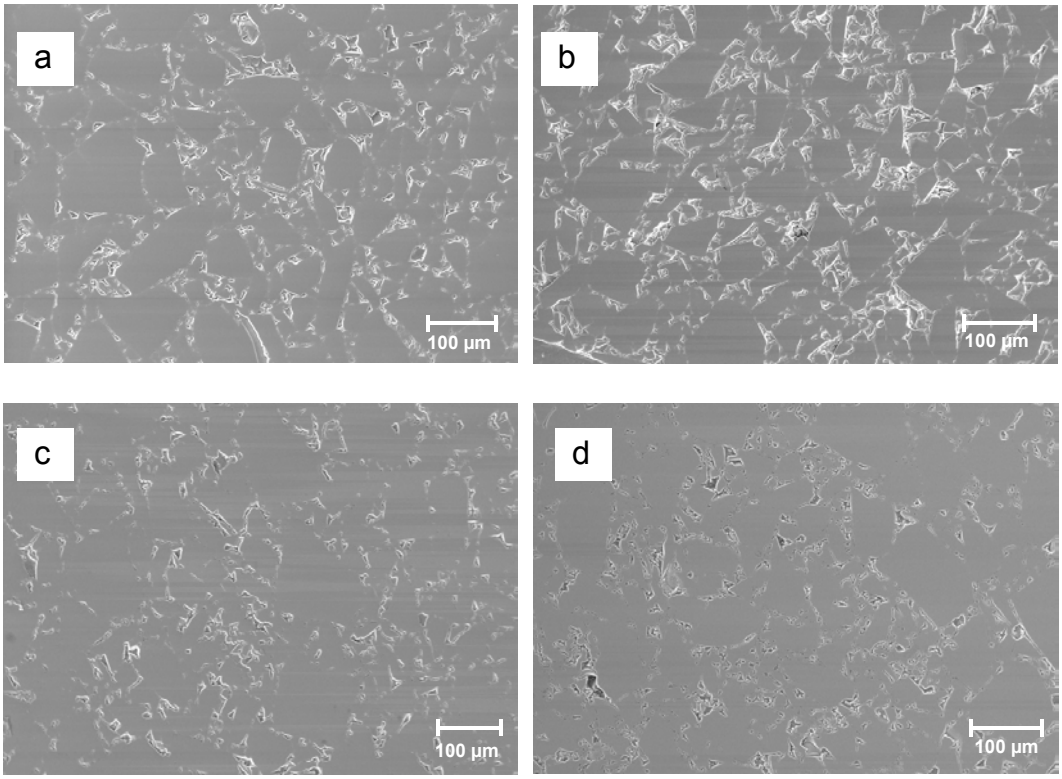

Figure: 3.4 Pore morphology and distribution in Si-B-C-N ceramics annealed at 1800 °C a) 1 h / 1 MPa (Sample I) (b) 3 h / 1 MPa (Sample II) (c) 1 h / 10 MPa (Sample III) (d) 3 h / 10 MPa (Sample IV).

(ii) Crystallization in pores/cracks

As indicated above, the annealed samples contain a large amount of pores in the size range of 2 µm – 10 µm. In the case of samples crystallized at high nitrogen overpressure (sample **IV**) these pores exhibit micrometer sized Si_3N_4 crystals. They seem to be nucleated at the pore surface and grown in to the pore volume (Figure 3.6). The crystals observed were found to have hexagonal morphology and were not observed to be formed elsewhere except in the

pores. Spot EDX measurements (Figure 3.8) of these micro-sized crystals indicate that they were Si_3N_4 crystals, however further structural information about these crystals needs to be investigated.

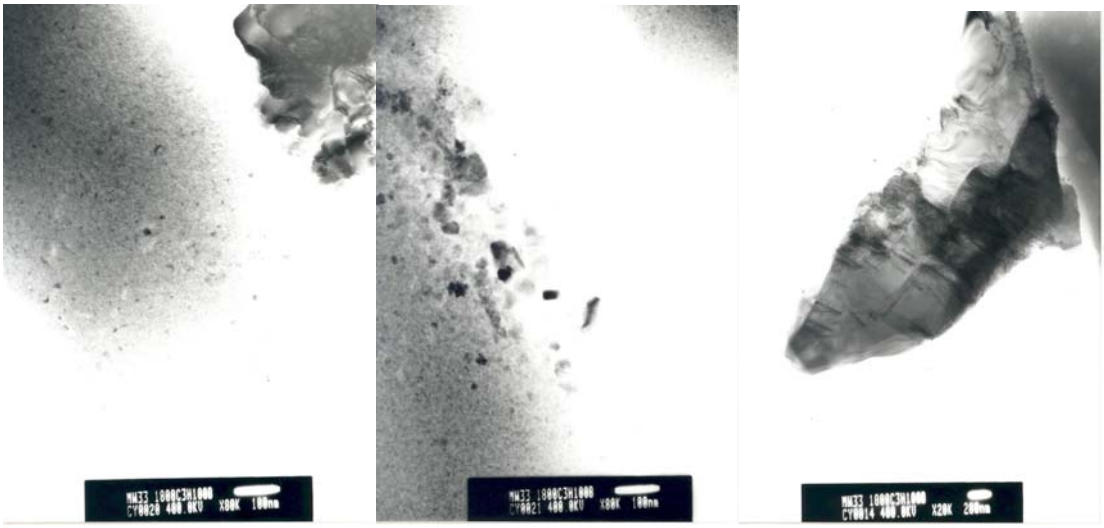

(a) **(b)** **(c)**

Figure: 3.5 Transmission electron microscopy of sample IV obtained at different places in the specimen exhibiting nano-crystallites whose size varies between 2 – 10 nm as seen in (a) and (b), along with crystallites of variant of α-Si3N4 phase which are as large as 200 nm and greater (c).

A high volume fraction of these crystals grow against each other, thus a steric hindrance of the grain growth and also a reduction in the aspect ratio occurs. The growth of the hexagonal basal plane of a crystal is stopped when it hits a prism plane of another crystal (Figure 3.6 (b) and (c)). This results in the impingement of a large amount of crystals, and one can observe such two or more crystals impinging each other and forming a network of crystals (Figure 3.6 (d)). Some of the impinged crystals are damaged or have some parallel cracks which can be attributed to the stresses that are generated in them (Figure 3.6 (d)). In any case the pores seem to be loosely packed by such crystals grown during annealing. Therefore the crystals may not influence strongly the creep flow in the surrounding microstructure.

In summary the material annealed at high nitrogen pressures 10 MPa. (sample **IV**) consists of a tri-modal distribution of the crystallites:

(a) Nano-crystallites of SiC and Si_3N_4 (as observed in TEM and also in SEM) - *of the order of 2 nm- 10 nm (Figure 3.5 (a) & (b) and Figure 3.6).*

(b) Large crystallites of a novel Si_3N_4 modification (discovered by Cai *et al.*) - *of the order of 200 nm and above (Figure 3.5 (c)).*

(c) Micrometre sized Si_3N_4 crystals in pores and cracks - *of the order of 2μm - 10μm (Figure 3.7).*

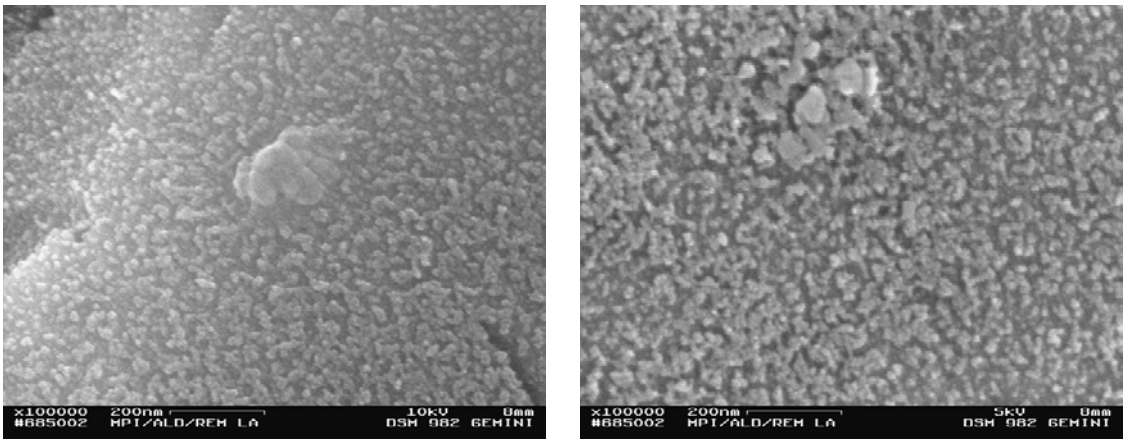

(a) **(b)**

Figure: 3.6 Nano-crystallites of SiC and Si_3N_4 can be observed in the material after plasma etching of the samples for 3.5 min.

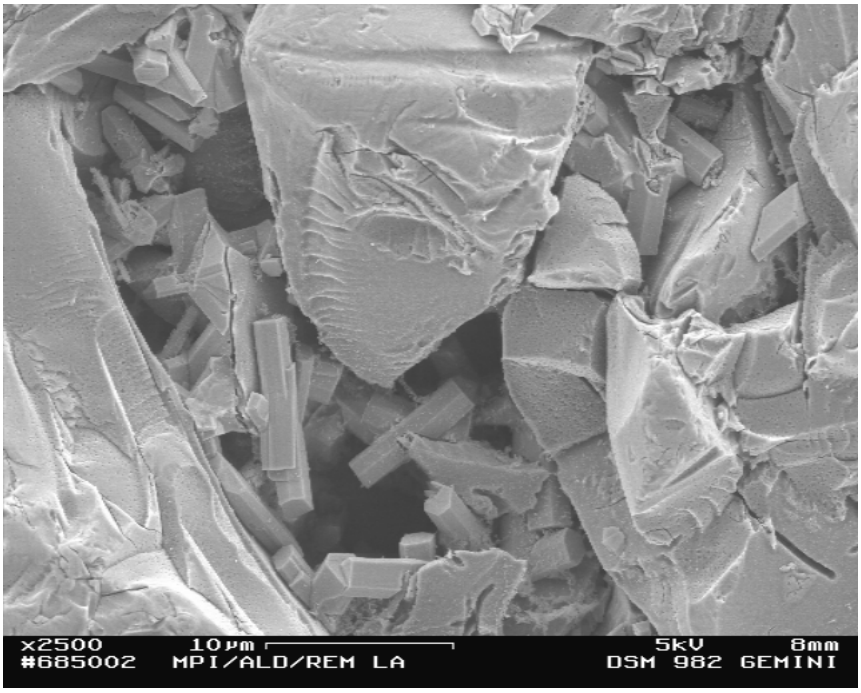

(a)

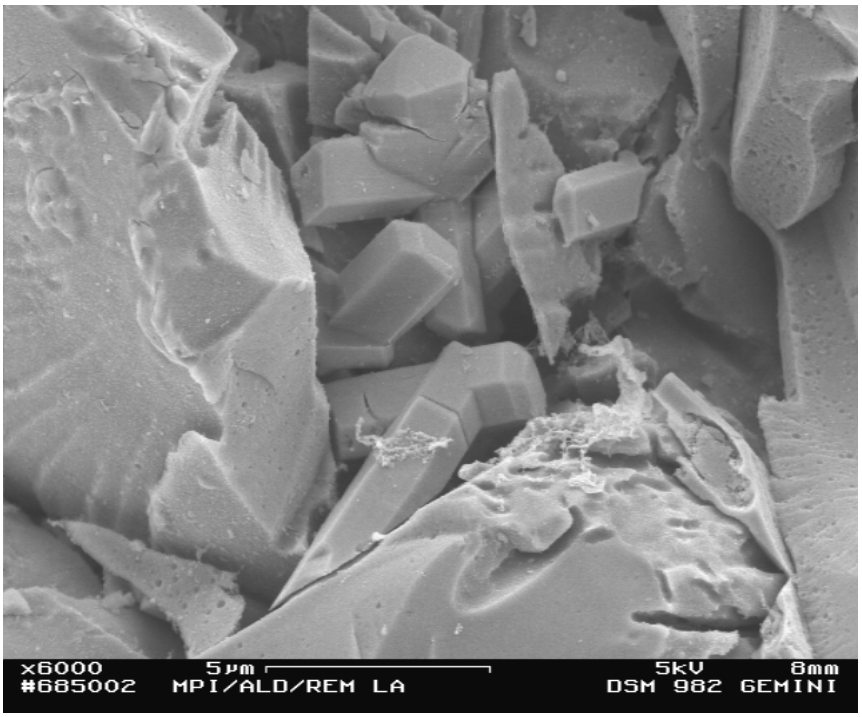
x6000 5µm 5kV 8mm
#685002 MPI/ALD/REM LA DSM 982 GEMINI

(b)

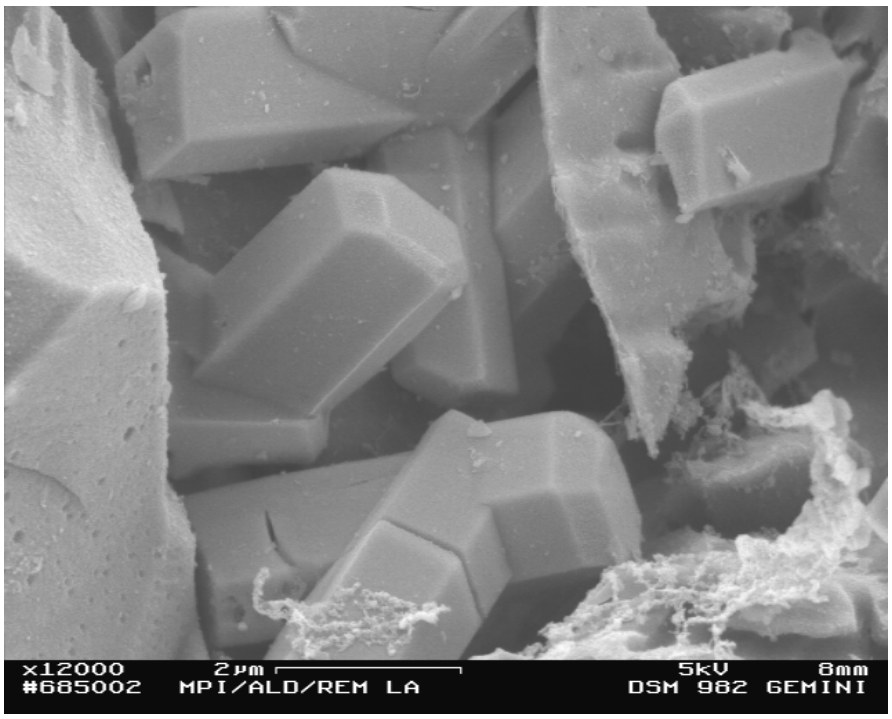
x12000 2µm 5kV 8mm
#685002 MPI/ALD/REM LA DSM 982 GEMINI

(c)

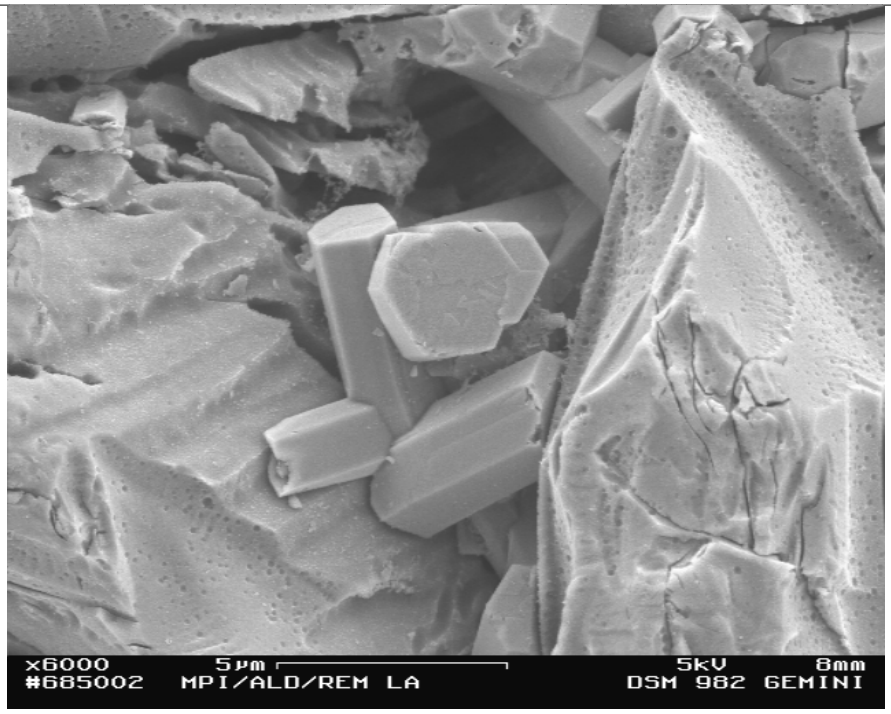

(d)

Figure: 3.7 Samples (sample IV) showing micrometer sized Si_3N_4 crystals with a hexagonal morphology inside the pores.

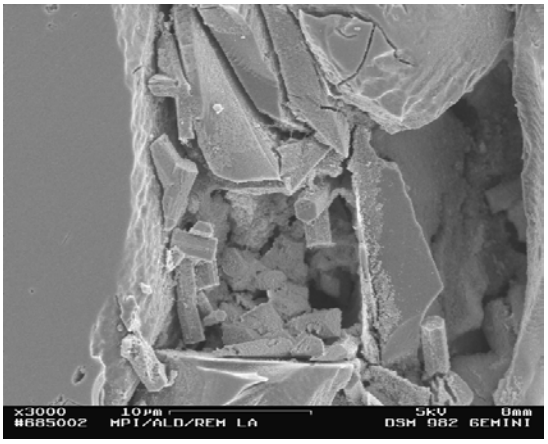

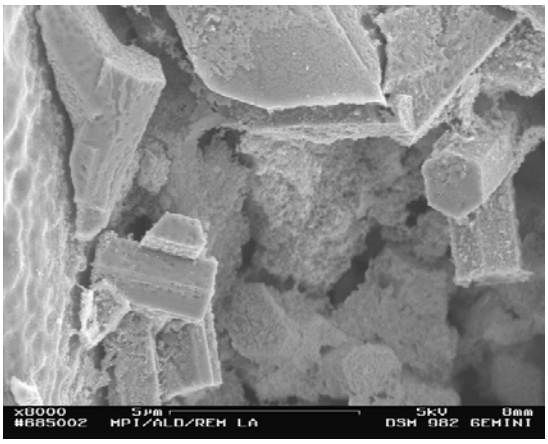

(a) **(b)**

Figure: 3.8 Damaged/overetched Si_3N_4 crystals observed in the pores of the material (sample IV) after a plasma etching time of 5 min.

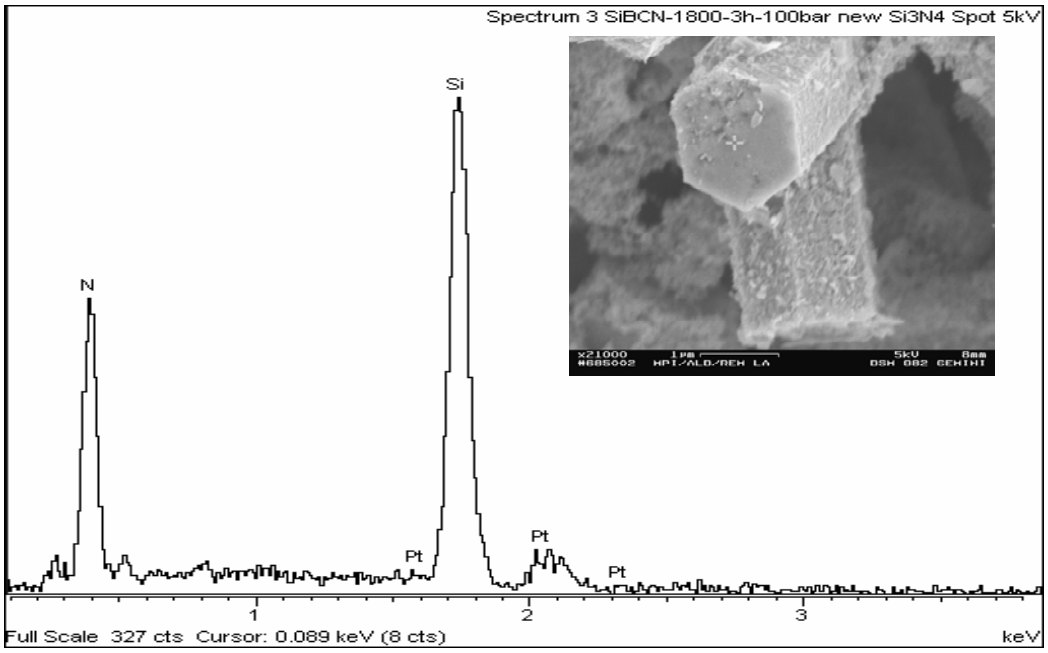

Figure: 3.9 Spot EDX of the micrometer-sized crystal in a pore shows Si and N peaks. Pt signal is seen due to the coating applied to the material before SEM observation.

3.1.3 Constant load experiments

Compression creep experiments were performed on the aforementioned as-thermolyzed and annealed Si-B-C-N specimens, and were done at a temperature of 1400 °C, and with a compressive load of 100 MPa. The results are summarized in Figure 3.10. In contrast to normal convention, in this figure the positive strain denotes compression in the direction of the applied load. The maximum deformation experienced by all the annealed samples was less than 0.75 % at the end of 300 h of creep time.

Since the deformation rates $\dot{\varepsilon}$ for all annealed Si-B-C-N samples were found within the experimental error to be almost indistinguishable (Figure 3.11 (a)), sample **II** has been selected as a representative material for further discussion and shown in Figure 3.11 (b) explicitly. According to the microstructural characterization this sample has the highest amount of crystallinity among the materials investigated. In Figure 3.11 (b) the strain rate $\dot{\varepsilon}$ of this sample is plotted along with that from the amorphous counterpart.

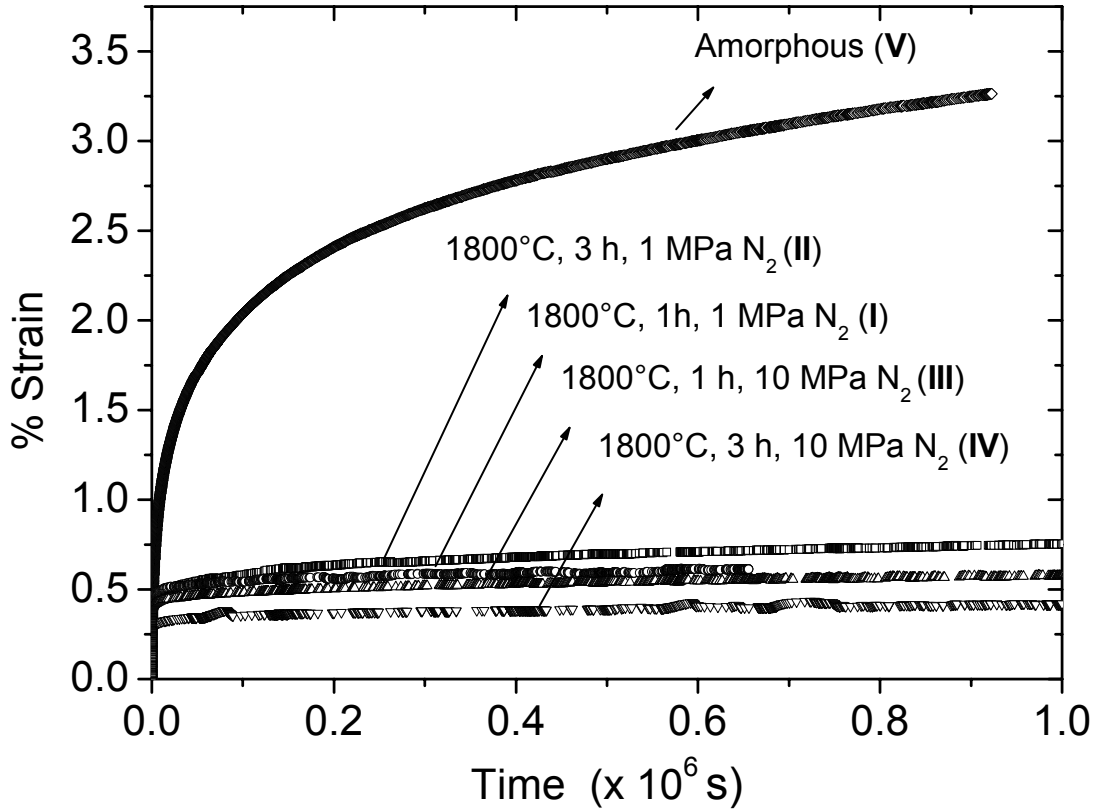

Figure: 3.10 Deformation (strain) of precursor derived amorphous and nano-crystalline Si-B-C-N ceramics at 1400 °C and a compressive stress of 100 MPa.

It can be seen that the time dependence of $\dot{\varepsilon}$ for the amorphous and nano-crystalline ceramics is similar, including the absence of any asymptotic behavior against a constant strain rate even after 300 h of testing time. However, there is a considerable difference in the magnitude of the strain rate between the annealed (nano-crystalline) and the amorphous Si-B-C-N sample, with the former showing a significantly higher creep resistance. For the crystalline material the deformation rates $\dot{\varepsilon}$ are about one order of magnitude smaller as for the amorphous counterpart, which holds for the whole testing time examined here. For the nano-crystalline ceramic the deformation rates $\dot{\varepsilon}$ decrease by about 2 ½ orders of magnitude reaching a value of 10^{-9} 1/s after 300 h.

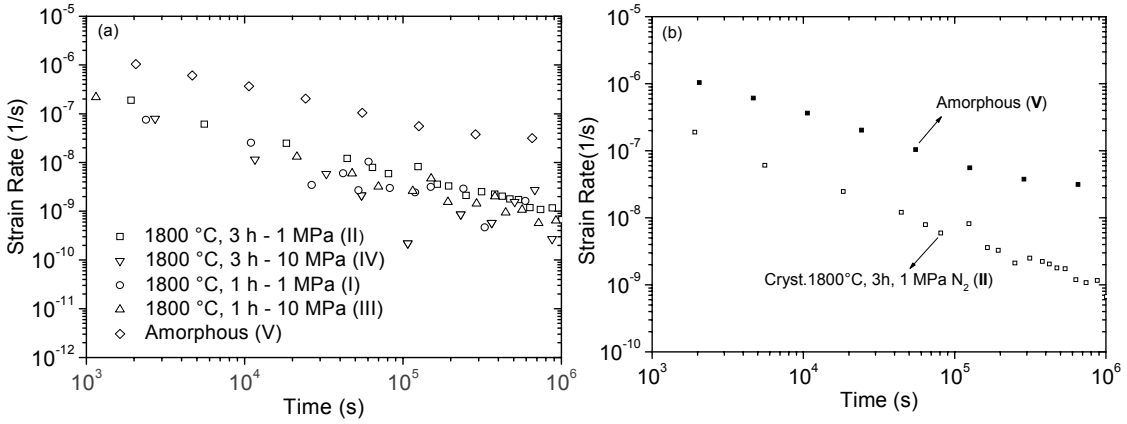

Figure: 3.11 Deformation rate (strain rate) of an amorphous Si-B-C-N ceramic (sample V) and nano-crystalline Si-B-C-N ceramics crystallized at 1800 °C for various holding times and pressures at a test temperature of 1400 °C and a load of 100 MPa.

3.1.4 Load change experiments

Additional compression creep experiments by applying various loads between 5 and 200 MPa during the particular time intervals given in Table 3.1 were performed for the aforementioned crystalline Si-B-C-N ceramics and the corresponding amorphous specimen. The dependence of the deformation for all samples as a function of increasing load (100 to 200 MPa) is shown in Figure 3.12 (a, b, c, d). Figure 3.12 (a) outlines the difference between sample **II** and the amorphous specimen.

At the end of creep testing the samples were unloaded from 200 MPa to 5 MPa, from which further information about the anelastic behavior in these materials was expected. The deformation rates $\dot{\varepsilon}$ for the crystalline Si-B-C-N ceramic (sample **II**) with compression loads, as derived from the curves in Figure 3.12 (a) are given in Figure 3.13.

Time (s)	Stress (MPa)
$0 - 2.5 \cdot 10^5$	100
$2.5 \cdot 10^5 - 5 \cdot 10^5$	150
$5 \cdot 10^5 - 9 \cdot 10^5$	200
$9 \cdot 10^5 - 1 \cdot 10^6$	5

Table: 3.1 Experimental conditions for load change experiments.

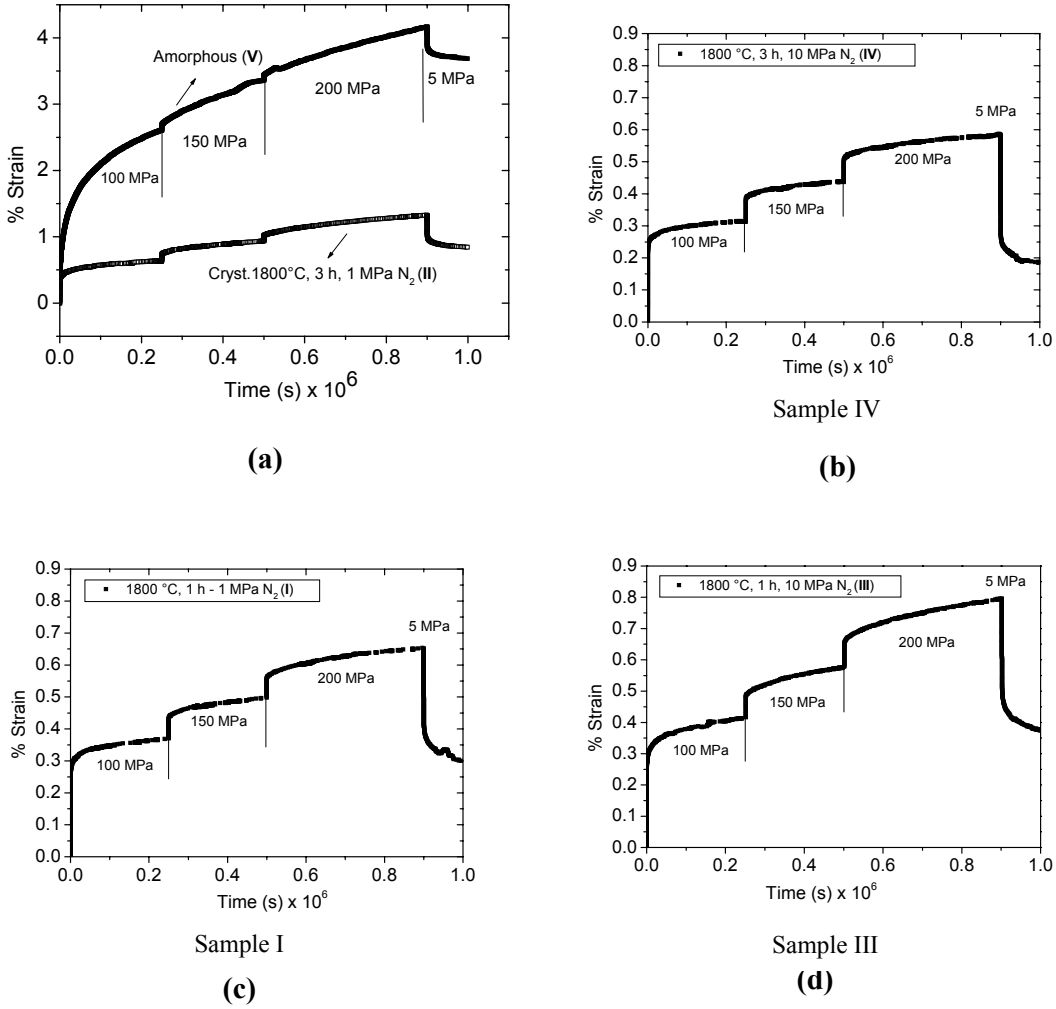

Figure: 3.12 Deformation (strain) as a function of time for an amorphous and differently annealed crystalline Si-B-C-N ceramics during a load change experiment at 1400 °C.

Inspection of the data in Figures 3.12 and 3.13 reveals that the deformation rates continue to decrease even after 300 h of testing time which holds for the amorphous and nano-crystalline ceramics as for all applied loads. The strain rate $\dot{\varepsilon}$ of the crystallized material can be approximated by Equation 3.1, which was applied earlier for the description of strain rate curves from amorphous precursor-derived ceramics [00Chr, 00Chr1]

$$\dot{\varepsilon} = \frac{1}{a + bt} \ . \tag{3.1}$$

In this equation, t represents the creep time, while a and b denote fitting parameters.

Viscosity is a property of materials, which is a measure of resistance to flow. When the shear stress varies linearly with the shear strain rate, the flow is considered to be Newtonian.

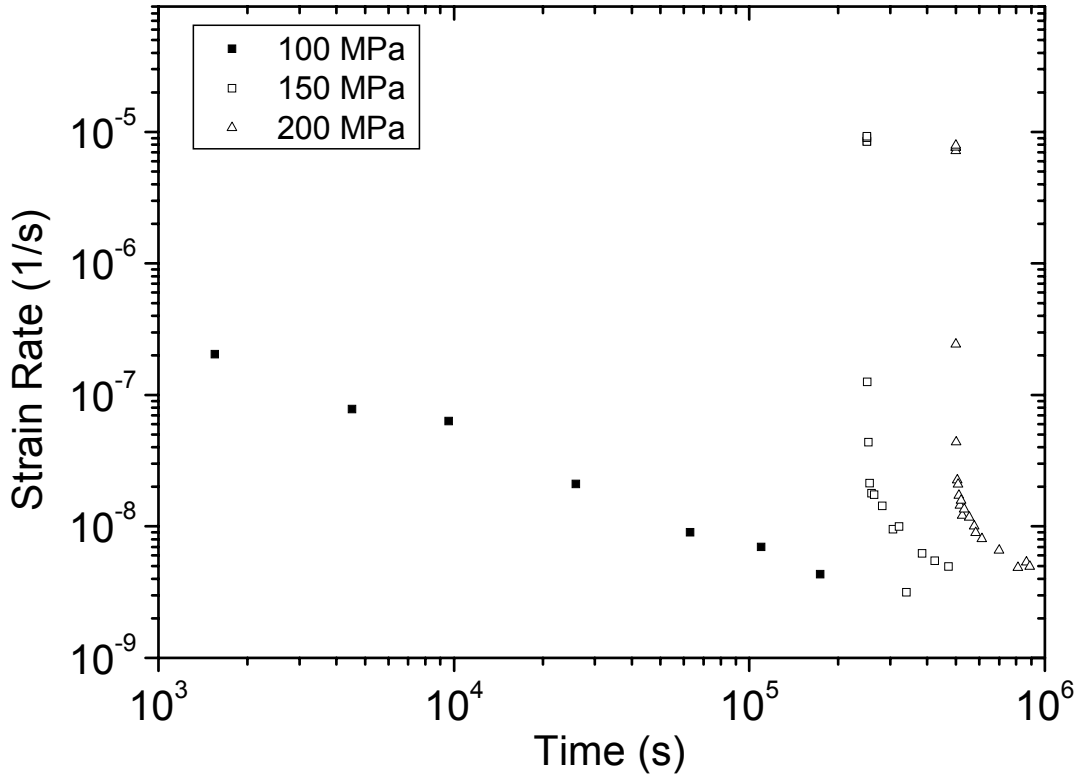

Figure: 3.13 Deformation rate (strain rate) as a function of time for a nano-crystalline Si-B-C-N ceramic crystallized at 1800 °C, 3 h – 1 MPa N_2 overpressure (sample II) during a load change experiment at 1400 °C.

The Newtonian viscosity is given by the equation

$$\eta = \frac{\sigma}{2(1+\nu)\dot{\varepsilon}} \cdot \tag{3.2}$$

Accordingly the viscosities of the present ceramic materials were determined by plotting the deformation rates $\dot{\varepsilon}$ as a function of applied stress σ, and assuming Newtonian viscous flow (see Figure 3.14).

The values of the deformation rates $\dot{\varepsilon}$ for various loads (i.e., stresses σ) at an identical time of $t = 10^6$ s were obtained by extrapolation of the data given in Figure 3.12. The viscosity η is calculated by means of Equation 3.3, which approximates Equation 3.2 when poisson's ratio for precursor derived ceramics is assumed to be ν = 0.25:

$$\eta = \frac{\sigma}{3 \cdot \dot{\varepsilon}} \ . \tag{3.3}$$

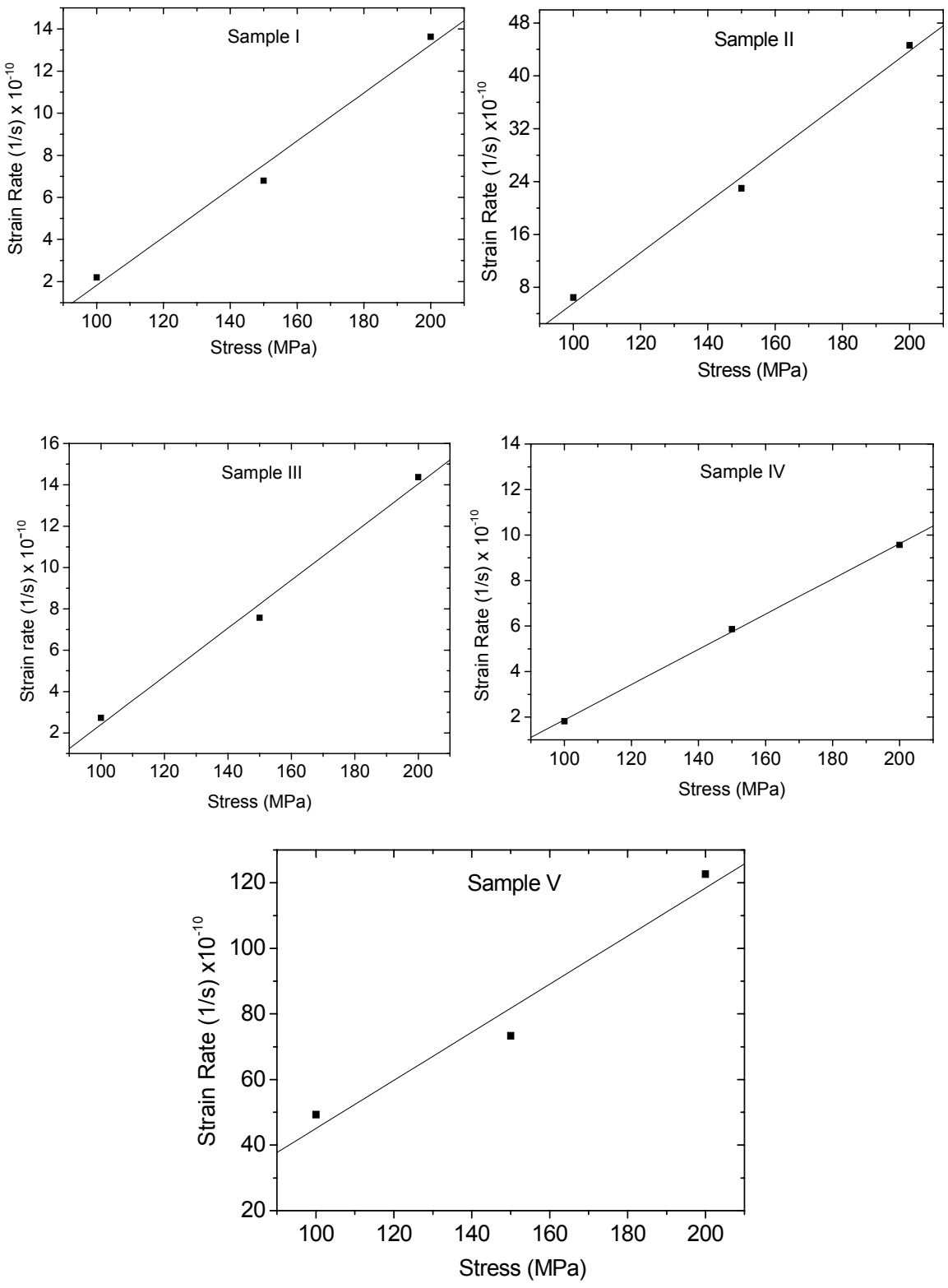

Figure: 3.14 Determination of Newtonian viscosity for amorphous (sample V) and nano-crystalline Si-B-C-N ceramics (Samples I, II, III, IV & V).

Material Condition	Viscosity
Amorphous	4.50×10^{15} Pa·s
1800 °C, 3 h, 10 bar N_2 (**II**)	8.72×10^{15} Pa·s
1800 °C, 3 h, 100 bar N_2 (**IV**)	4.31×10^{16} Pa·s
1800 °C, 1 h, 10 bar N_2 (**I**)	2.96×10^{16} Pa·s
1800 °C, 1 h, 100 bar N_2 (**III**)	2.86×10^{16} Pa·s

Table: 3.2 Viscosity data obtained from creep strain rate measurements at 1400 °C using Equation 3.3.

This analysis provides Newtonian viscosities of 10^{15} to 10^{16} Pa·s for the amorphous Si-B-C-N ceramic and nano-crystalline samples, respectively, which refer to the testing temperature of 1400 °C (Table 3.2). The increase of the viscosity by crystallization of the as-thermolyzed material is moderate which is in contrast to the findings, for instance, in metallic glasses [80Pat, 80And, 98Wai].

3.1.5 Comparison of crystalline materials

The Figure 3.15 shows a comparison of the behavior of materials annealed under low (1 MPa) and high nitrogen overpressure (10 MPa), referred to as sample **II** and sample **IV** respectively at 1400 °C. Although the crystallinity of sample **II** is higher than that of sample **IV** the strain is higher than that of the material which contain less amount of crystalline phases according to the microstructural characterization. As can be seen in Figures 3.15 to 3.17 this is true at all loads (100 – 200 MPa) and at all temperatures (1300 °C, 1350 °C and 1400 °C) investigated, i.e., the nano-crystalline Si-B-C-N ceramics produced under high nitrogen overpressures exhibited the least deformation at any condition.

Load change experiments for sample **II** at 1350 °C, yield an instantaneous elastic strain of around 0.363 % at an initial load of 100 MPa, which decreases to around 0.114 %, at 150 MPa and 200 MPa respectively. With the reduction of the final load of 200 MPa to 5 MPa, around 0.423 % of the elastic strain is recovered and an accumulated viscous strain of 1 % is recorded.

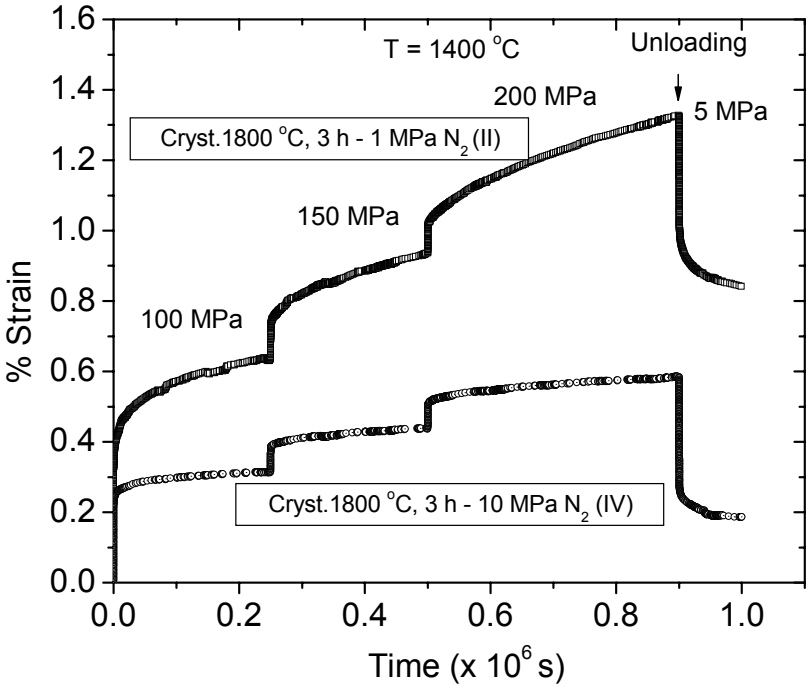

Figure: 3.15 Load change experiments for nano-crystalline Si-B-C-N ceramics. The nano-crystalline ceramic produced under high nitrogen overpressure exhibits the least deformation at all loads.

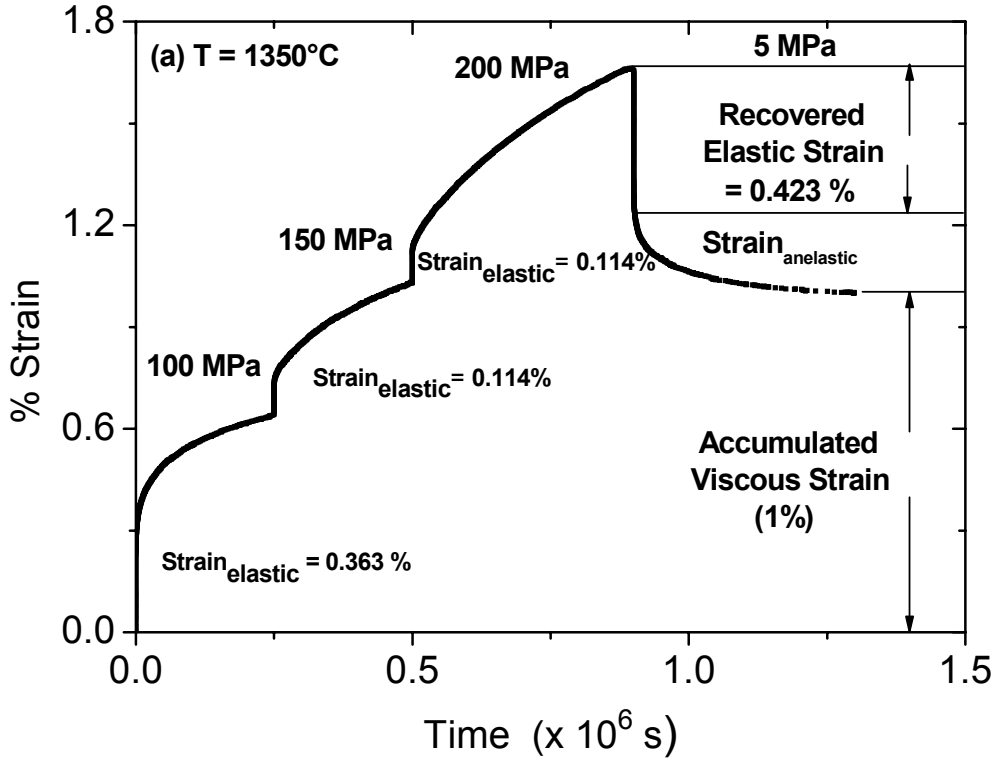

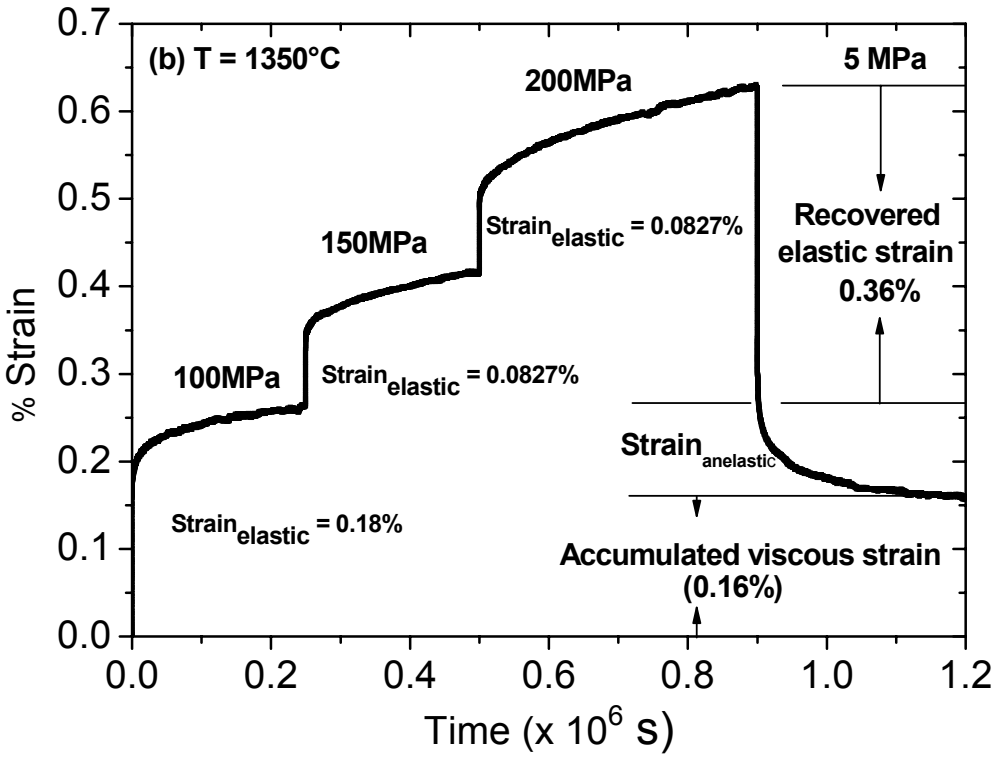

Figure: 3.16 Comparison of nano-crystalline Si-B-C-N ceramics (annealed at 1800 °C for 3 h) produced under (a) low pressure (1 MPa) (sample II) and (b) high pressure nitrogen environment (10 MPa) (sample IV).

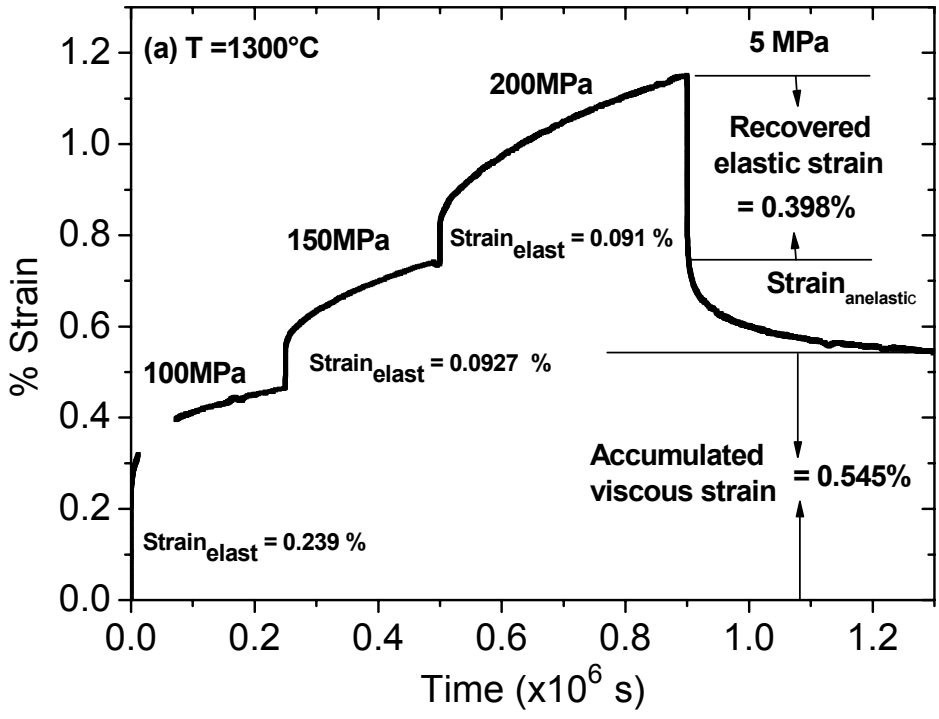

(a)

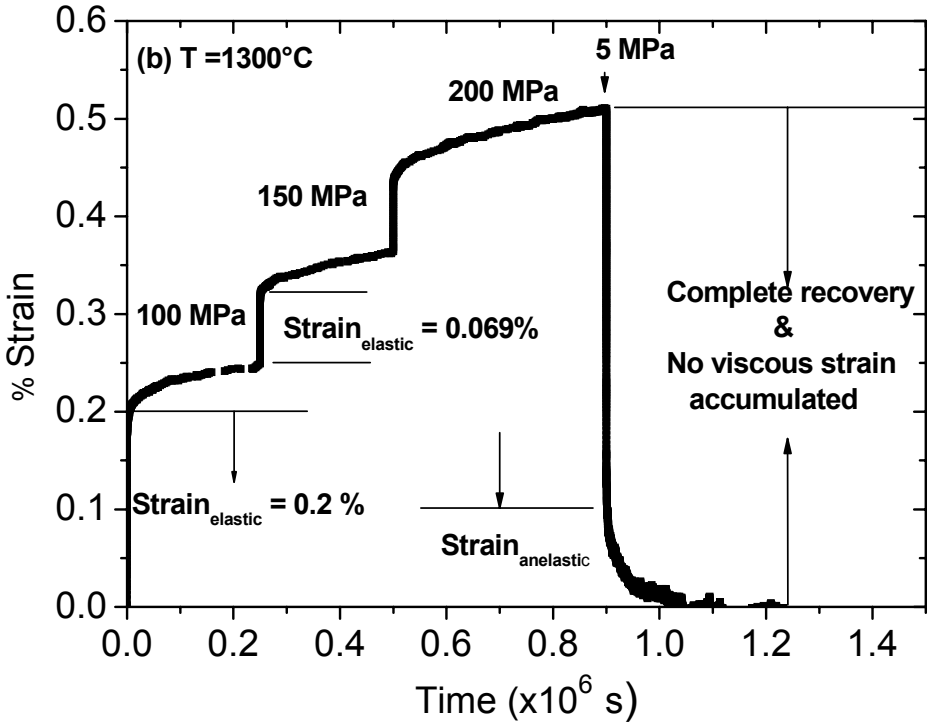

(b)

Figure: 3.17 Comparison of nano-crystalline Si-B-C-N ceramics produced under (a) low pressure (1 MPa) (sample II) and (b) high pressure nitrogen environment (10 MPa) (sample IV). (b) shows complete recovery at 1300 °C, indicating apparently no accumulation of viscous strain.

For sample **IV**, at 1350 °C an instantaneous elastic strain of 0.18 % at 100 MPa and subsequently, increments of 0.0827 % at 150 MPa and 200 MPa are recorded. On unloading the sample, an elastic recovery of 0.36 % is recorded. Finally, as the material is allowed to relax until the strain becomes constant, a viscous strain of 0.16 % is accumulated in the material.

Experiments at 1300 °C for sample **II** show an instantaneous elastic strain of 0.239 % upon application of 100 MPa, and subsequently elastic strain increments of 0.0927 % at 150 MPa and 200 MPa. An elastic strain of around 0.398 % is recovered instantly when the sample is unloaded and an accumulated viscous strain of 0.545 % is recorded. Sample **IV,** on the other hand, exhibits an instantaneous elastic strain of around 0.2 % at 100 MPa, and subsequently, increment values of 0.069 % at 150 MPa and 200 MPa. Upon unloading, it is observed that

there is complete recovery of the strain and there is no sign of any accumulation of viscous strain in the material at the end of 300 h of testing time. At 1300 °C, sample **IV** is distinguished by its apparent lack of any plastic deformation.

3.1.6 Anelasticity

If during a load experiment the load on the specimen is released, then a finite time is required to establish equilibrium between stress and strain in the unloading direction. The resulting time-dependent reversible deformation, which also depends on the applied initial stress, is termed anelastic. In fact, such an anelastic deformation was observed earlier for amorphous precursor-derived Si-B-C-N ceramics [94Chr]. Unloading experiments were performed for the present materials by reducing the final load from 200 to 5 MPa as the last step in the load change experiments already discussed (see Figure 3.12). The time dependence of the anelastic strain rates for the amorphous and nano-crystalline Si-B-C-N ceramics (sample **II**) is given in a double logarithmic representation in Figure 3.18.

The experimental data given in Figure 3.18 were fitted using the well-known Kohlrausch-Williams-Watts (KWW) equation, which has been frequently used for the description of relaxation processes in various materials [47Koh, 92Tei, 92Che, 87Kak, 93Böh]. According to this approach, the relaxation for a residual strain ε(t) is described by Equation 3.4:

$$\dot{\varepsilon} = \frac{d\varepsilon(t)}{dt} = -\gamma(t) \cdot \varepsilon(t) \,. \tag{3.4}$$

The time dependence of the coefficient γ(t) is assumed by

$$\gamma(t) \approx t^{-(1-\beta)}, \text{ with } 0 < \beta \leq 1. \tag{3.5}$$

The analytical solution of Equation 3.5 is known as the stretched exponential or Kohlrausch-Williams-Watts function [47Koh]. The anelastic strain ε_{an} (t,T) is then given by

$$\varepsilon_{an}(t,T) = \varepsilon_0 \exp\left[-\left(\frac{t}{\tau_{rel}(T)} \right)^{\beta} \right] \cdot \tag{3.6}$$

The parameter τ_{rel} in Equation 3.6 denotes an effective relaxation time, while the stretching exponent β quantifies the extent of the deviation from pure exponentiality, or equivalently, the degree of relaxation time dispersion. The KWW function implies a spectrum of relaxation times whose width is connected with the parameter β. A stretching exponent β of 1 thus describes a relaxation process with single activation energy (infinitesimally sharp relaxation spectrum), while the relaxation spectrum broadens to an large number of activation energies for values of β close to zero [86Sch]. The time derivative of Equation 3.6 yields the anelastic strain rate $\dot{\varepsilon}_{an}$, defined as,

$$\dot{\varepsilon}_{an}(T,t) = -\frac{\varepsilon_0 \beta}{t} \cdot \left(\frac{t}{\tau_{rel}(T)} \right)^{\beta} \exp\left[-\left(\frac{t}{\tau_{rel}(T)} \right)^{\beta} \right]. \tag{3.7}$$

This latter equation was used to fit the experimental anelastic strain data for the amorphous and nano-crystalline Si-B-C-N ceramics, depicted in Figure 3.18. The derived values of ε_0, β, and τ_{rel} for both samples are summarized in Table 3.3. It can be seen that the data for both materials are very similar. The ε_0 value is identical and the relaxation time τ_{rel} in both systems are around $3 \cdot 10^4$ s. Only the parameter β is somewhat different indicating that the nano-crystalline Si-B-C-N ceramic implies somewhat sharper relaxation time dispersion.

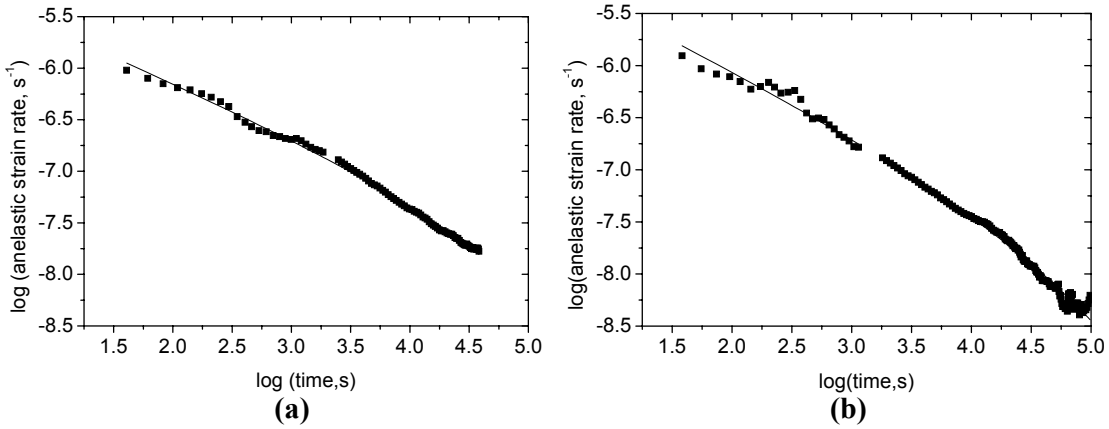

Figure: 3.18 Investigation of anelasticity using Kohlrausch William Watts equation for (a) amorphous Si-B-C-N ceramic (sample V) (b) crystallized Si-B-C-N ceramic (sample II).

Material	Amorphous Si-B-C-N	Cryst. Si-B-C-N
ε_0	$2.5 \cdot 10^{-3}$	$2.6 \cdot 10^{-3}$
β	0.50	0.41
τ_{rel} [s]	$2.8 \cdot 10^{4}$	$3.6 \cdot 10^{4}$

Table 3.3 Derived parameters from stress strain measurements (analysis with KWW equation, see text)

3.2 Discussion

3.2.1 Sample annealing, crystallization and structural characterization

Amorphous Si-B-C-N ceramics are metastable with respect to the formation of the crystalline phases silicon nitride, silicon carbide, carbon and boron nitride [00Pen]. However, interestingly, the metastable state of these materials is quite stable due to the low atomic mobility, and they crystallize at rather high temperatures. If such amorphous materials are annealed at high temperatures, then various processes may alter the structure, which comprise densification, crystallization and phase separation. Similar phenomena are observed in amorphous metallic glasses, when they are annealed at temperatures above the glass transition. The structural stability of these materials and thus, their mechanical properties may be substantially improved by crystallization. It has been shown that after crystallization, β-SiC and eventually Si_3N_4 nanocrystallites are embedded in a turbostratic "B-C-N" matrix consisting of amorphous carbon and boron nitride domains [01Chr]. Earlier studies on the crystallization of these materials indicated that in the temperature range between 1400 and 1500 °C silicon carbide is the first phase to nucleate, whereas silicon nitride nucleates massively only at and above 1700 °C [02Nar]. More recent high resolution TEM studies confirmed that the materials remain purely amorphous until 1300 °C, but first very small crystals (2 – 5 nm) of α - Si_3N_4 and β - SiC crystals were detected already at 1350 °C and 1400 °C respectively [01Cai]. However, it has to be stated that the Si_3N_4 crystals formed at

this low temperature are quite seldom and massive crystallization only occurs at substantially higher temperatures which is in agreement with the earlier findings.

It was observed that the crystallization kinetics directly depends on the actual annealing conditions. That is, the crystallization rate increases with increasing annealing temperature and time [02Nar]. Likewise, the gas atmosphere plays an important role as well, which in particular holds for the impact of a nitrogen atmosphere [02Cai]. For this reason samples of the amorphous Si-B-C-N ceramic were heat-treated under four different annealing conditions. The conditions (holding times, nitrogen pressure, and temperature) were chosen in such a way that neither Si_3N_4 decomposes nor the formation of Si_3N_4 is suppressed. In addition, it was tried to optimize these conditions in order to receive a Si-B-C-N specimen with a maximum of SiC and Si_3N_4 nanocrystals. The present X-ray diffraction, TEM and solid-state NMR data clearly demonstrate that a nitrogen pressure as high as 10 MPa stabilizes the amorphous state, i.e., retards the crystallization of SiC and suppresses the formation of Si_3N_4 nanocrystals. Likewise, extensive TEM studies have shown that holding times greater than 10 h at a given annealing temperature have only a marginal effect on the volume fraction of the produced nanocrystals [01Ald]. In general, a nitrogen pressure of 1 MPa was found to be completely sufficient to stabilize Si_3N_4 crystals. It was further concluded that an increasing nitrogen pressure provides no benefit, since it only retards the crystallization processes. Thus for the present situation, an annealing temperature of 1800 °C, a holding time of 3 h, and a nitrogen pressure of 1 MPa were found to be the optimum conditions for the preparation of a Si-B-C-N specimen with a maximum of SiC and Si_3N_4 nanocrystals. These conclusions are confirmed by both the X-ray diffraction and the TEM data.

Moreover, the derived results from the solid-state NMR investigation are in full agreement with the aforementioned X-ray diffraction and TEM data. It should be noted that so far no solid-state NMR studies exist for the structural evolution of Si-B-C-N ceramics after being subject to different annealing conditions at such high temperatures. In general, it is found that

the present ^{29}Si NMR and ^{13}C NMR experiments provide consistent results. At such high annealing temperatures of 1800 °C, in principle, two basic processes have to be distinguished: (i) sample decomposition via the reaction of Si_3N_4 with "free" (amorphous) carbon to form SiC and nitrogen [00Pen], and (ii) devitrification of the amorphous ceramic material, i.e., demixing of the amorphous "Si-C-N"-matrix along with the formation of crystalline Si_3N_4 and SiC domains [00Pen, 01Ald, 01Bil]. For the present discussion the demixing process is obviously dominant, since sample decomposition is largely suppressed at a nitrogen pressure of ≥ 1 MPa. The same is also understood from the carbon activity vs. temperature diagram (Figure. 1.1) as discussed in section 1.2.3.

Thus, the experimental ^{13}C and ^{29}Si NMR spectra prove the presence of SiC (^{29}Si NMR signal at -18 ppm, ^{13}C NMR signal at 20 ppm), amorphous carbon (^{13}C NMR signal at 120 ppm), and Si_3N_4 (^{29}Si NMR signal at -48 ppm). For all cases, the spectral intensity of the SiC component is somewhat larger than that of the Si_3N_4 component, which qualitatively fits with the X-ray observations. The NMR results for specimen **II**, i.e., increase of the silicon carbide signal, loss of amorphous carbon signal, and reduction of silicon nitride signal intensity, might indicate the presence of some decomposition during sample annealing as well. However, it could well be that the ^{29}Si NMR signal intensities are not completely correct, since in purely crystalline Si_3N_4 very long spin-lattice relaxation times are expected, which for experimental reasons cannot always be accounted for. Much more important, however, is the considerable reduction of the ^{29}Si NMR line widths, which obviously stems from an enhanced degree of crystallinity of sample **II**.

The highest degree of crystallinity thus is registered also with NMR for the sample exposed to a nitrogen pressure of 1 MPa at 1800 °C for 3 h (sample **II**). At the higher nitrogen pressure of 10 MPa, silicon carbide and silicon nitride domains are formed as well. However, relatively broad ^{29}Si NMR line widths are registered, reflecting a lower degree of crystallinity of these samples. It is also possible that the broad ^{29}Si NMR is indicative of the mixed

coordinated SiC_xN_y ($x \neq 4$, $y \neq 4$) domains. In agreement with the corresponding X-ray diffraction and TEM studies, the present solid-state NMR data show that, the highest degree of crystallinity is achieved by applying longer annealing times and lower nitrogen pressures. On the basis of the ^{11}B NMR data it can be concluded that during the silicon carbide formation and sample crystallization distinct changes occur in the co-ordination sphere of the boron atoms. That is, a certain amount of the boron nuclei, that originally built up hexagonal BN domains, change their coordination from trigonal to tetragonal. Similar observations have been made during a previous NMR study on this precursor system where the samples were annealed in an argon atmosphere [01Sch]. However, so far no further information about the constitution and structural changes within these BN domains is available.

3.2.2 Mechanisms of formation of Si_3N_4 crystals in a high pressure nitrogen environment

The mechanisms of formation of micrometer-sized silicon nitride crystals in precursor derived ceramics annealed at 10 MPa nitrogen overpressure is interesting to investigate. Micrometer sized α-Si_3N_4 were observed in Si-C-N materials by Kleebe *et al.* [98Kle] earlier in pores and cracks in addition to nano-crystallites of SiC and Si_3N_4. Micrometer-sized SiC also was observed by the aforementioned authors. It was argued that crystallization in Si-C-N materials on inner and outer surfaces leads to two different results. First, crystallization at accessible surfaces proceeds by thermally induced decomposition of the amorphous Si-C-N phase, yielding a Si-C enriched material since molecular nitrogen escapes the system which is a quasi-open system. These Si-C enriched regions crystallize to the corresponding thermodynamically stable phases β-SiC and carbon. Second, an additional crystallization process may proceed via vapor phase reactions of the gaseous decomposition products with the formation of idiomorphic (having proper form or shape) α-Si_3N_4 at inner surfaces of the cracks/pores. This is expected to happen in the quaternary Si-B-C-N system also, and the hence the formation of Si_3N_4 crystals in the pores of the material.

3.2.3 Mechanical deformation at high temperatures

During the present work two types of high temperature compression tests were performed at a working temperature of 1400 °C, namely constant load experiments and load change experiments. The constant load experiments, with a load of 100 MPa, were performed on four different annealed Si-B-C-N samples, and for comparison on an amorphous Si-B-C-N specimen. In general, an extraordinarily high creep resistance could be detected for both types of materials. However, the deformation rate for the crystallized Si-B-C-N ceramics was found to be an order of magnitude lower as that of the amorphous material throughout the whole testing period, implying a smaller total deformation of crystallized materials (Figure 3.11). It therefore can be concluded that a higher creep resistance emerges from sample crystallization. However, this is questionable since the material of sample **IV** which reveals according to the characterization data the lowest amount of crystallinity shows the highest creep resistance among the materials investigated (which was also evident from the less amount of accumulated viscous strain in sample **IV** after load change experiments, Section 3.1.5).

The time dependence of the deformation rate for the amorphous and nano-crystalline Si-B-C-N ceramics (Figure 3.11) can be understood on the basis of a continuous structural evolution of the matrix phase during such experiments. Since the time dependence is rather similar, it is reasonable to assume that the matrix plays the dominant role for the deformation behavior even of the crystalline Si-B-C-N ceramic rather than the dispersed crystallites. In close analogy to the amorphous sample [00Chr], the ongoing structural changes in the amorphous matrix with testing time result in an increase of viscosity and a densification which are mainly responsible for the continuous reduction of the deformation rate of the partially crystalline ceramics.

The role of the amorphous matrix phase in the reduction of the strain rates in as-annealed materials can be elucidated by careful consideration of the strain rate curves as shown in Figure 3.19 (a) and Figure 3.19 (b).

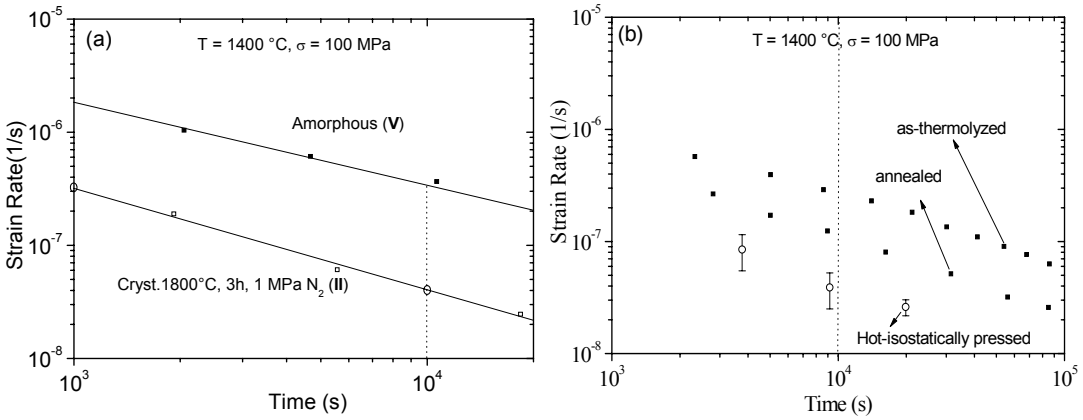

Figure 3.19 Strain rate as a function of time for as-thermolyzed and annealed Si-B-C-N ceramics heat treated at (a) 1800 °C for 3 h (~ 10^4 s) (b) 1400 °C for 80 h (00Chr) tested under identical conditions of load and temperature.

Annealed sample heat treated at 1800 °C for a duration of 3 h (~ 10^4 s) in a nitrogen atmosphere yields a strain rate value of 4 x 10^{-8} s^{-1} at 10^4 s under the creep conditions as indicated in the figure. Since the time dependence of the strain rates was linearly decreasing, a strain rate value of 3 x 10^{-7} s^{-1} was obtained at 10^3 s by extrapolation. Strain rate corresponding to 10^4 s for the as-thermolyzed amorphous sample (without any heat treatment) was ~ 3.4 x 10^{-7} s^{-1}, which was close to the extrapolated value obtained for the crystalline sample at 10^3 s. This indicates that the amorphous specimen during this annealing time of 10^4 s would reach strain rate values to that of the crystalline specimen at the start of the creep test. This is a direct evidence for the reduced creep rates in annealed samples as a result of the structural changes and densification of the amorphous matrix phase, where the role of the crystallites is considered to be of minor importance.

Figure 3.19 (b) shows the time dependency of the deformation rate of a sample after thermolysis, annealing (heat treated at 1400 °C for 80 h and HIPing (hot isostatic pressing). Earlier findings by Christ *et al.* [00Chr] have indicated that heat treatment of the MW-33 ceramic matrix at a temperature as low as 1400 °C in nitrogen atmosphere for an increased holding time of 80 h, increases the pore-free density to $\rho_{ann} \approx 2.47$ g/cm^3. A similar increase in the pore-free density of the MW-33 ceramic matrix is observed after HIPing (hot isostatic

pressing) at 1600 °C and 200 MPa for 4 h resulting in $\rho_{HIP} \approx 2.56$ g/cm^3, the findings of which are indicated in Figure 3.19 b. Consequently, it was concluded that the increase in ceramic matrix density leads to an improvement in the creep resistance of the material. Hence an increase in creep resistance and also the time dependence of strain rates of the annealed samples, could be explained by the densification of the matrix phase.

The presence of isolated nanocrystallites obviously plays a minor role for the time dependence of the deformation or creep rate. This is in contrast to the observations for partially crystalline metallic glasses where the effect of crystallization dominates the creep behavior [80Pat]. The creep rates were found to decrease by several orders of magnitude in annealed metallic glasses, where continuous crystallization was observed in prolonged creep experiments at high temperatures. The strong reduction of the creep rate from its initial value was mainly attributed to the *in situ* formation of crystallites in such metallic glasses. It was further observed that the creep rates of completely crystalline specimens do not drop down any further, and reach a constant limiting value [80Pat]. In the case of the present annealed Si-B-C-N ceramics, the structural evolution of the amorphous phase is not completed even after three hours of annealing at 1800 °C. Thus, structural changes in the amorphous B-C-N matrix still go on during the entire time of the creep experiments. This is also consistent with the absence of any asymptotic approach to steady state even after 300 h of testing time. The fact that the crystallization rate in Si-B-C-N ceramics is much smaller than in metallic glasses also supports the hypothesis of a minor influence of the nanocrystallites embedded in the amorphous phase on the enhanced creep resistance of the annealed Si-B-C-N ceramics. A finite contribution from the nanocrystallites, nevertheless, cannot be completely ruled out.

The viscosity values of amorphous and nano-crystalline Si-B-C-N ceramics derived from load change experiments were found to be close to 10^{15} and upto 10^{16} Pa·s respectively at 1400 °C which are up to more than eight orders of magnitude higher than the values ~ 5 x 10^8 Pa·s discussed for fused silica at the same temperature [76Kin] which proves the high mechanical

stability of the more covalent Si-B-C-N materials against the more ionic oxidic glass at these temperatures. Figure 3.20 (a) summarizes the viscosity data available in the literature for Si-C-N ceramics, Si-B-C-N ceramics, both in amorphous and crystalline states. They are compared to those of fused silica [76Kin] as a function of temperature. Also a value is typical for high creep resistant liquid phase sintered polycrystalline Si_3N_4 [95Lue] is given. The lower line of the data field referred to for earlier findings at MPI is the viscosity due to the initial creep strain and the upper line to the strain rate after 10^6 s of creep testing. The substantial decrease of the strain rate with time of creep testing was found to be mainly due to the change i.e., the relaxation of the amorphous structure.

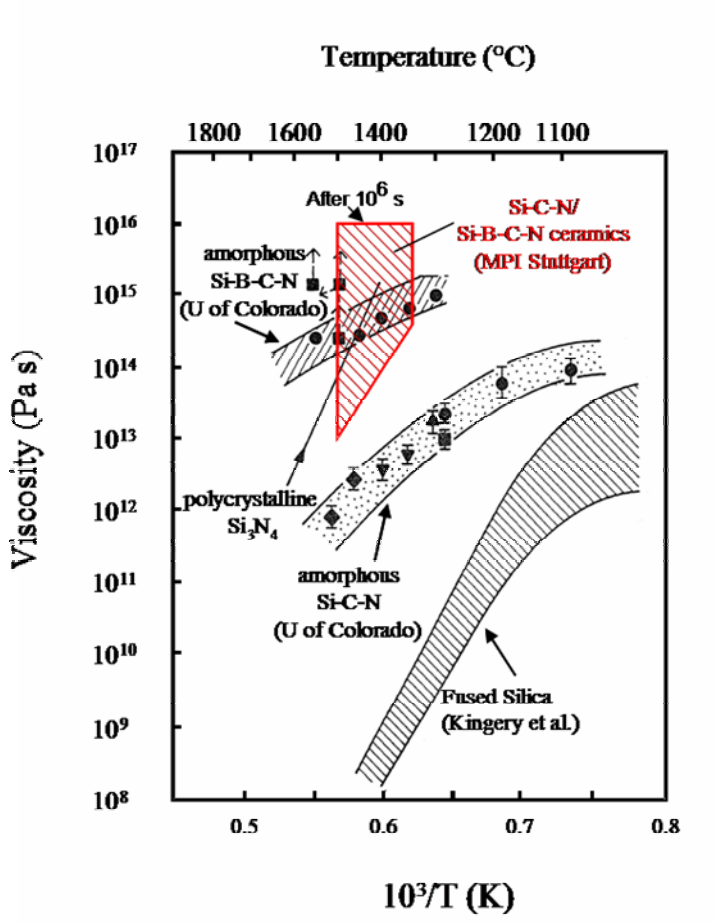

Figure: 3.20 (a) Comparison of viscosities of amorphous and crystalline (synthesized at MPI Stuttgart [00Chr and present work]) Si-B-C-N ceramic materials with fused silica and polycrystalline Si_3N_4 as a function of temperature. Data from Rishi Raj's group (University of Colorado, Boulder) has been included for comparison [98Lin, 98Rie], a typical value for polycrystalline Si_3N_4 is represented as dotted line [95Lue], and data for fused silica taken have been taken from Kingery *et al.* [76Kin].

The viscosity values derived in this work from load change experiments (Table 3.2) and constant load experiments (Figure 4.14) are plotted in Figure 3.20 (b) together with the data field of the earlier findings in the institutAlthough the values are dependent strongly on the processing conditions, the reported values are in consistency each other. It should be pointed out that the highest values of viscosity reported for crystalline Si-B-C-N ceramics obtained from MW-33 precursor was calculated after 300 h (~ 10^6 s) of testing time when the strain rate values were still showing decreasing trend with no asymptotic approach to constant values indicating that the creep resistance can be even more increased by further heat treatments i.e., the strain rate levels well below 10^{-9} s^{-1} at 1400 °C.

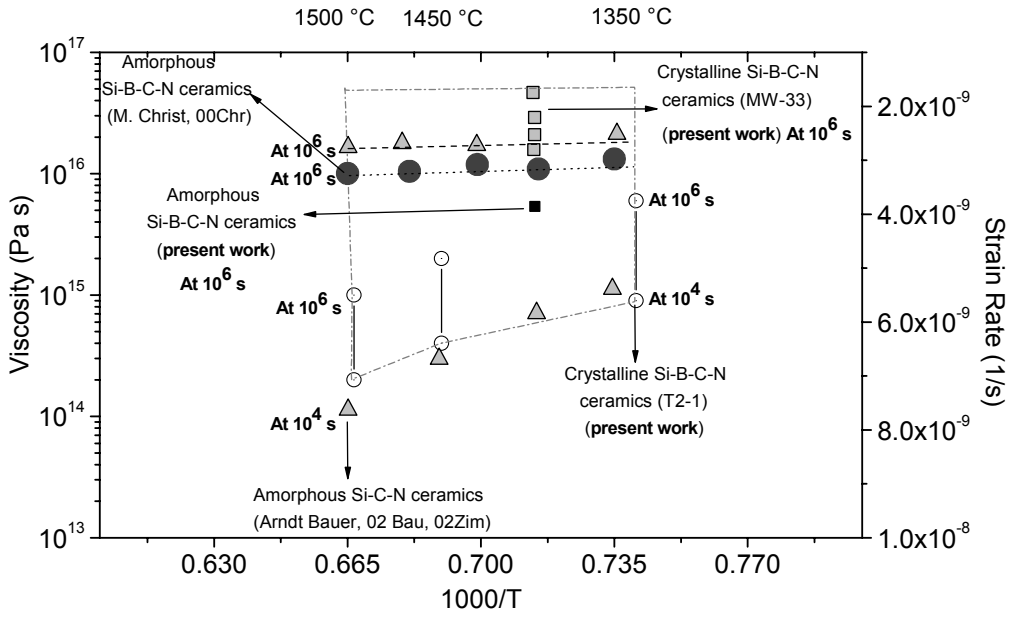

Figure: 3.20 (b) Calculated viscosity values obtained from load change experiments of crystalline Si-B-C-N ceramics (MW-33 precursor) at a temperature of 1400 °C in comparison with crystalline Si-B-C-N ceramics (T2-1 precursor) between 1350 °C - 1500 °C at 50 MPa. Viscosity values from amorphous Si-C-N and amorphous Si-B-C-N ceramics from previous investigations from the institute are also plotted.

(△ = Amorphous Si-C-N ceramics, ■ = Crystalline Si-B-C-N ceramics (MW-33), ● = Amorphous Si-B-C-N ceramics, ○ = Crystalline Si-B-C-N ceramics (T2-1)).

Earlier experiments have indicated that, for longer times, the deformation rate in the load change experiments approaches the respective values observed under constant load, although the total deformation in the load change experiment is much smaller than under a constant

stress of 50, 100 or 200 MPa [02Zim]. As a consequence, it can be concluded that the deformation rate and the related viscosity at a given time depend on the annealing time but not on the load history. This eliminates the possibility of ambiguities in the viscosity values plotted in Figure 3.20 (b) where the values from the load change and constant load experiments are plotted together.

3.2.4 Comparison of deformation behavior with differently annealed materials

In this section, the differences in the high temperature deformation behavior of crystalline ceramics obtained at low and high N_2 pressures (1 MPa and 10 MPa), identified as sample **II** and sample **IV,** respectively, are discussed based on the accumulated plastic strain in the materials after load change experiments.

From previous experience with constant load experiments it is clear that even after 300 h of testing at 1400 °C, both materials exhibited only primary creep with no asymptotic approach to steady state (Figure 3.15 – 3.17). The parallel trend in the strain rates to be seen in Figures 3.15 – 3.17 indicate that even in the partially crystallized samples (that are investigated here), the amorphous matrix phase still dominates the creep behavior of this composite type of material. The constitutive equation for the high temperature deformation in the primary creep regime can be written as

$$\varepsilon_t = \varepsilon_e + \varepsilon_{an} + \varepsilon_v , \qquad (3.8)$$

where, ε_t = total strain, ε_e = elastic strain, ε_{an} = anelastic strain, ε_v = viscous strain.

It should be noted that the components of anelastic strain and viscous strain are functions of stress (σ), time (t), temperature (T) and the material itself. The viscous strain is the total plastic deformation accumulated in the material at the end of the creep test after the load release after a duration of 300 h of creep time.

As both the samples were annealed at 1800 °C, before creep testing on the one hand the crystallinity of the samples is not likely to increase remarkably during creep at temperatures

between 1300 °C – 1400 °C, hence the possibility of influence of crystallization during creep on the high temperature deformation is not likely. On the other hand, however, the pretreatment at 1800 °C will cause a structural evolution of the amorphous matrix phase for both the materials. The following arguments are placed to reason out why a material produced at high nitrogen pressures (sample **IV**) experiences less plastic deformation compared to the material produced at relatively low N_2 pressure (sample **II**). However, the time dependence of deformation for both the materials is similar.

High nitrogen overpressure during the processing of sample **IV** results in suppression of crystallization to a large extent except for favoring the formation of some minor nanocrystalline α-silicon nitride (2 – 5 nm) in the matrix [01Cai, 02Cai], and the formation of micrometer sized silicon nitride in pores and cracks of the material (discussed in Section 3.1.2). Microscopic investigations revealed that the micrometer sized Si_3N_4 crystals were not found to exist elsewhere in the material other than pores. Therefore, these crystals do not play any role in the deformation process. From the XRD scans, it is evident that sample **IV** has still a lot of residual amorphous phase in the material where as sample **II** was crystallized much stronger. Hence sample **IV** is considered to be structurally similar to an amorphous Si-B-C-N ceramic, but annealing at 1800 °C results in an increased density of the matrix. Table 3.4 lists the values of the weight of the samples before and after creep.

Temperature	**Cryst. 1800 °C, 3h - 1 MPa N_2**			**Cryst. 1800 °C, 3 h - 10 MPa N_2**		
	Mass before creep (mg)	Mass after creep (mg)	% mass gain	Mass before creep (mg)	Mass after creep (mg)	% mass loss
1300 °C	48.10	48.70	1.25	84.90	84.5	0.47
1350 °C	52.50	53.10	1.14	74.80	74.0	1.07
1400 °C	59.98	60.20	0.366	69.63	58.8	15.55

Table: 3.4 Weight gain and weight loss of samples after load change experiments at 1300 °C, 1350 °C and 1400 °C.

A noticeable difference between both samples was observed as there was a mass gain after creep of specimens produced from sample **II** at all temperatures which is attributed to oxidation. On the contrary, the specimens produced from sample **IV** showed a weight loss.

Earlier studies by Christ *et al.* [01Chr] on the high temperature deformation behavior of crystallized Si-B-C-N ceramics showed that the total deformation was composed of two components, namely, a strain component which is dependent on the applied stress and a component independent of the applied stress which differs significantly from that of the amorphous material. It was shown that the volume of the amorphous material decreases at high temperature due to annealing of the free volume, and that the volume of the crystallized material expands during exposure to high temperatures in air. The effects of internal oxidation and elimination of free volume are superimposed to the creep deformation. Obviously, both the effects tend to cancel each other.

In contrast to amorphous ceramics which formed a passivating oxide layer on the surface, the crystallized ceramics in this study showed oxidation also inside the specimen (though not so significant) which is able to explain for the mass increase during exposure to air during the creep experiments at elevated temperatures. The oxidation also gives rise to a volume increase which reduces the apparent creep deformation. Sample **IV** has a predominantly amorphous character, and hence there is less oxidation-induced volume increase. However, the load release experiment shown in Figure 3.16 (b) suggests that zero viscous strain is accumulated in sample **IV.** This would again hint at a strong concurrent volume increase during deformation, but in contrast to sample **II,** a mass loss rather than a mass gain occurs during creep. The fact that this mass loss becomes unusually very high at 1400 °C (shown in Table 3.4) may provide a hint about the nature of the decomposition reaction which occurs. However, it was not possible to completely resolve this question within the framework of this thesis.

3.2.5 Anelastic response

Earlier studies showed that the fitting parameters β and τ_{rel} (Equation 3.7) seem to be independent of the applied stress, while the pre-exponential constant ε_0 exhibits a pronounced stress dependence, which is reflected by a linear variation with stress change [02Bau]. In the present study, no further attempts were made to relate these fitting parameters to the applied stress. The stretching exponent β is known to be directly connected with the structural relaxation of these materials.

Stretching exponents of β = 0.6 for amorphous $Ni_{0.5}Zr_{0.5}$ [92Tei], β = 0.43 for C_{60} [92Che], β = 0.42 for amorphous silicon [87Kak], β = 0.4 – 0.6 for various polymers [93Böh], and β = 0.47 for amorphous Si-C-N ceramics [02Bau] have been reported in literature. It should be noted that the stretching exponent is between 0.4 – 0.6 in most of the cases. Phillips *et al.* [94Phi, 95Phi] tried to explain the stretching exponent by a trap model, which is based on the idea that, in glasses there exists a static distribution of traps or sinks towards which excitations diffuse and disappear [82Gra]. The value of the stretching exponent is then given by

$$\beta = \frac{d}{(d+2)}, \tag{3.9}$$

where d is the dimensionality of the configuration space in which the relaxation takes place. For a 3-dimensional distribution, Equation 3.9 leads to a value of β = 0.6 which explains the stretching exponents observed for some of the glasses, but not for all materials. Considering the long range forces, namely, the Coulomb forces, a dimensionality of d = 3/2 was derived and this assumption leads to the stretching exponent β = 3/7 = 0.43 which is much closer to the value which has been observed for the crystalline Si-B-C-N ceramic investigated (Table 3.3). According to this model, Coulomb forces would govern the observed relaxation processes in addition to density fluctuations. Furthermore, for amorphous Si-B-C-N ceramics the stretching exponent β = 0.5 is neither close to 0.43 nor 0.6. It should be noted that the

stretching exponent for stress relaxation in oxide glasses is also of the order of 0.5, for a wide range of compositions [86Sch]. With this, the model proposed by Phillips might not be applicable to all materials in general, thus requiring a need for a more generalized formulation which could accommodate all materials.

To summarize, the MW-33 derived crystallized materials exhibit strain rates which continuously decrease with time (similar to amorphous materials) but on a lower level (an order of magnitude lower) which can be attributed to the densification of the matrix phase, and the structural change of the amorphous phase as a result of annealing. Though all the annealed materials showed an order of magnitude increase in creep resistance, a closer look at the results indicated that the annealed material synthesized at higher nitrogen pressures exhibited the least accumulated viscous deformation.